Modelling the structural loading of a small wind turbine at a highly turbulent site via modifications to the Kaimal turbulence spectra

Amir Bashirzadeh Tabrizi[*a], Jonathan Whale[a], Thomas Lyons[b], Tania Urmee[a], Joachim Peinke[c]

[a] *Physics and Energy Studies, School of Engineering and Information Technology, Murdoch University, Perth, WA 6150, Australia*

[b] *Environmental Science , School of Veterinary and Life Sciences, Murdoch University, Perth, WA 6150, Australia*

[c] *ForWind—Center for Wind Energy Research, Institute of Physics, Carl von Ossietzky University of Oldenburg, Oldenburg, Germany*

Abstract

Although, wind turbines have traditionally been sited in open terrain, there is a growing trend of installing turbines in non-homogeneous terrain, such as urban areas. Recorded urban turbine failures suggest that turbine design has been inadequate for the turbulence experienced at these sites and hence a better understanding of the turbine-loading issues in the built environment is required.

This paper compares turbine blade load statistics for inflow turbulence fields based on the open terrain standard Kaimal spectra, as suggested in the standard IEC61400-2 that covers the design and safety standard of small wind turbines, and measured turbulence spectra from a built environment site. The findings show that for extreme, high turbulent intensity winds, the measured spectra predict isolated loading events around twice the magnitude of loads predicted by use of the standard spectra. The work suggests the need for improvements to the standard in order to model the non-Gaussian wind statistics that occur in extreme events such as sudden strong gusts.

Keywords: Small wind turbines, IEC61400-2, Kaimal spectra, Built environment, TurbSim, FAST.

Nomenclature

I	Turbulence intensity [-]
σ_1	Standard deviation of longitudinal wind speed [m/s]
σ_m	Standard deviation of measured wind speed [m/s]
σ_s	Standard deviation of simulated wind speed [m/s]

* Corresponding author; Tel.: +61893606713; E-mail: a.btabrizi@murdoch.edu.au.

I_{15}	Characteristic turbulence intensity at 15 m/s [-]
a	Slope parameter for turbulence standard deviation model [-]
V_{hub}	Mean wind speed at the hub-height of the turbine [m/s]
L_k	The velocity component integral scale parameter [m]
k	Index for the velocity component direction (i.e. 1 = longitudinal, 2 =lateral, and 3 = vertical) [-]
z	Height of the anemometer a.g.l [m]λ
h	Height of the Bunnings warehouse façade a.g.l [m]
U(t)	Wind speed time series [m/s]
λ^2	Intermittency parameter [-]
τ	Time lag [s]
$U_\tau(t)$	Wind speed increment time series for time lag τ [m/s]

1. Introduction

Wind turbines have traditionally been designed for rural areas over open terrain. There has, however, been an increasing trend towards the installation of wind turbines in non-open terrain, such as in urban areas, above forests and in mountainous regions[1, 2]. The drivers for this change in turbine location include the search for new sites now that prime sites have already been taken, and the increased use of turbines in urban areas as part of a reaction to increasing electricity prices and a desire for energy independence[3]. For example, within the last 5 years in the metropolitan area of Perth, Australia, there have been installations of 400W Maglev wind turbines for lighting on tree-lined promenades and at busy ports; 3kW Maglev turbines near large shopping centres; 1kW Urban Green Energy wind turbines in car parks near 5-star Green star buildings, and 1.5kW Swift wind turbines on top of a hardware warehouse building in a commercial suburb. In addition to these local examples, there are several international examples such as turbines installed at peri-urban sites e.g. on education campuses, ranging in size from 1kW to 5kW. Some of the small machines installed in the built environment have suffered structure failure, which has led to wind turbines receiving bad publicity[4]. In an extreme case in Hobart, Australia, police cordoned off the street when the blades of a building mounted turbine collapsed in on themselves in strong winds due to ultimate load failure after over-speeding[5].

Many of these non-open sites are often characterised by highly turbulent wind flow and the literature suggests that there is a direct correlation between high turbulence intensity of wind and increased fatigue and reduced life of wind turbines[6, 7]. High turbulence is a strong candidate as a possible reason for the aforementioned structural failures of machines at urban sites[8]. Certainly it is likely that the turbines were not specially designed for operation in the built environment since the current IEC international design standard IEC6400-2: Wind turbines – Part 2: Small wind turbines (ed. 3) is based on open terrain and does not include design models for such highly turbulent sites[9, 10].

The IEC6400-2 standard mandates designers to use a Normal Turbulence Model (NTM) that describes turbulence and turbulence intensity and includes the effects of varying wind speed and varying direction[10]. IEC6400-2 defines a 'characteristic turbulence intensity, *I*, as the 90th percentile of turbulence intensity measurements binned with respect to wind speed[10]. For each wind speed bin, the 90th percentile value of *I* is obtained by taking the mean *I* value in the bin plus 1.28 standard deviations of *I* from the mean, thus assuming a Gaussian distribution for turbulence intensity values. The Normal Turbulence Model (NTM) states that the expected standard deviation of longitudinal wind speed, σ_1, is given by the following equation based on data collected from open terrain sites[10]:

$$\sigma_{1(90\%)} = I_{15}(15 + aV_{hub})/(a + 1) \quad (1)$$

where

a = 2 and I_{15} = 0.18. Therefore Eq. 1 can be rewritten as:

$$\sigma_{1(90\%)} = I_{15}(0.67V_{hub} + 5) \quad (2)$$

It is important to note that this equation was developed by Stork *et al.* and is based on observations of hub-height, 10-minute average wind speeds in the range 10-25 m/s over open terrain[11]. Figure 1 shows the standard deviation of longitudinal wind speed versus mean wind speed, 5.95 metres above the rooftop of a hardware warehouse building in the suburb of Port Kennedy, Perth, Western Australia, and is based on ten day's worth of measured 10-minute averaged data. The dashed line in Figure 1 is a linear fit of the 90th percentile of measurements of standard deviation of longitudinal wind speed binned with respect to wind speed. For each wind speed bin of measured data, the 90th percentile value of σ (longitudinal wind speed) is obtained by taking the mean σ value in the bin plus 1.28 standard deviations of σ from the mean. The slope and intercept of the fitted line is 0.24 and 0.23 respectively. Therefore, an equivalent "IEC equation" based on measured data is as below:

$$\sigma_{1(90\%)} = I_{15}(1.33V_{hub} + 1.28) \tag{3}$$

The IEC61400-2 predicted relationship from Eq. 1 has been added to the figure for comparison. The figure supports the argument that Eq. 1 does not represent the measured data in the built environment since the relationship that the standard uses is for open terrain and for wind speeds in the range of 10 m/s – 25 m/s. The equivalent equation resulting from measured data in the urban environment has a bigger slope and smaller intercept compared to the IEC equation. Figure 1 shows the bulk of the data is at lower wind speeds and this is expected of an urban area. Turbulence levels are also expected to be higher in the urban area and this is the case in the plot for higher wind speeds. Eq. 1 over-predicts turbulence levels for wind speeds below 7 m/s and under-predict turbulence levels for wind speeds above 7 m/s. Wind direction and building geometry may have an influence here, with low turbulence, low wind speeds from some directions and high turbulence, high wind speeds from others.

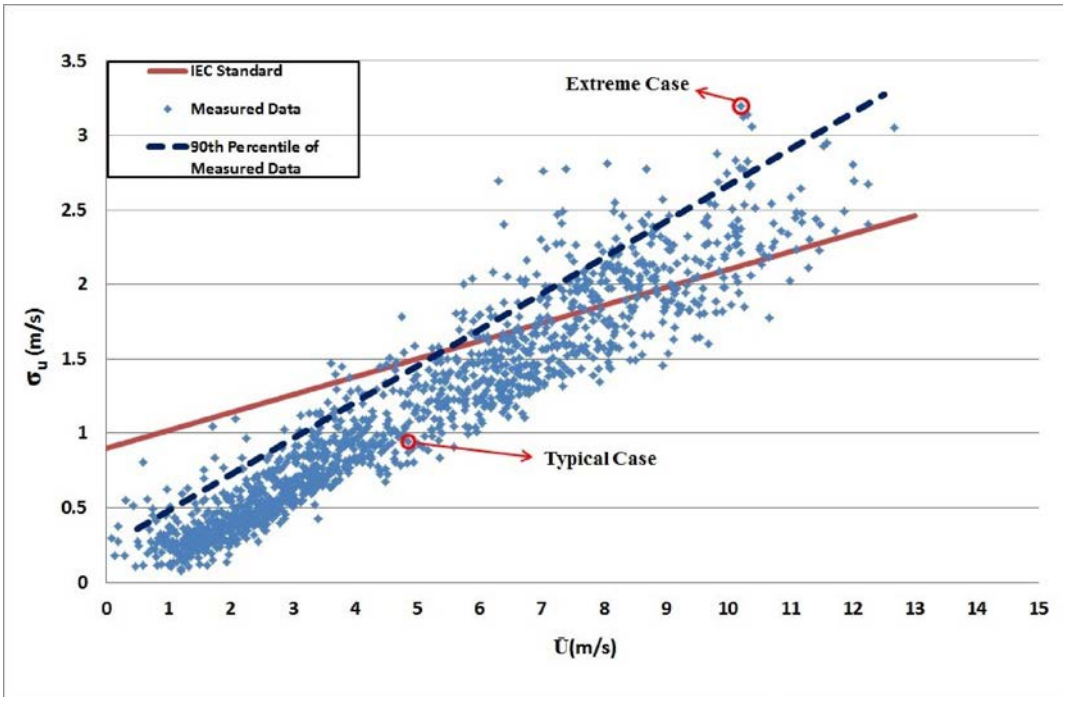

Figure1. Standard deviation of longitudinal wind speed versus mean wind speed, 5.95 metres above the rooftop of a warehouse building in the suburb of Port Kennedy, Perth, Western Australia

Wind turbine designers use aero-elastic models incorporating the NTM to predict the loading on turbines. Calculations using these models, sometimes in combination with tests, are used to determine the ultimate and fatigue strength of the structural components of the wind turbine. It is important to distinguish between fatigue, which is a gradual compromise of structural component integrity over time, and ultimate loads that occur when structural properties e.g. maximum material strength, are exceeded. Given that the NTM has been developed for open terrain sites, the research question of this paper is, how accurate are the aero-elastic models in predicting the loading on turbines in non-open terrain?

A considerable body of literature has investigated various load cases and fatigue loading on wind turbine blades. Many of the articles have focussed on the analysis of large wind turbine blades from turbines in open terrain sites especially in terms of application composite materials in blade design[12-14]. Some researchers have studied the structural and fatigue loading of large and medium wind turbines installed in highly turbulent locations, such as in complex terrain or in the wake of an upstream wind turbine. They investigated how different parameters such as surface roughness, atmospheric instability, wind speed, turbulence intensity, turbulence length scale etc., can affect loading and fatigue on turbines operating in such high turbulent locations[15-17].

The impact of atmospheric and wake turbulence on wind turbine fatigue loading was investigated by Lee *et al.*[15] using large-eddy simulations of atmospheric boundary layers under various stability and surface roughness conditions. They found fatigue loads increased with surface roughness but atmospheric instability had minimal influence. Furthermore, downstream turbines experienced higher fatigue loads indicating that the turbulent wakes generated from the upstream turbines had a significant impact. Thomsen and Sorensen[16] found that the increased fatigue loading in a wind farm compared to free flow is between 5% and 15%, depending on the wind farm layout. Noda and Flay[17] discovered that a reduction in lifetime by a factor of about 2 occurs between a low wind speed, low turbulence intensity site, compared to a high wind speed, high turbulence intensity site for a horizontal axis wind turbine. Botta *et al.*[18] confirmed that harsh climatic conditions and complex terrain could affect both the energy output and the steady and fatigue loading on wind turbines. They suggested that a critical appraisal of present design procedures is needed as far as hostile terrain is concerned.

Mouzakis *et al.*[19] showed that wind turbulence structure is the main fatigue causing parameter for all wind turbine components. Furthermore, the fatigue loading on turbines in complex terrain is increased compared with flat terrain and in some cases this increase can exceed 30%,. Riziotis and Voutsinas[6] found that the main driving fatigue mechanism in complex terrain is turbulence intensity. The authors suggest that small length scales and strong three-dimensionality of the inflow, which are characteristic of complex terrains, are secondary factors for increasing the fatigue loads but can be significant in some cases. Their results also confirm the significance of yaw misalignment on wind turbine loading.

Several researchers have used different wind models to simulate 3D wind fields across the rotor and compare fatigue loads of wind turbines. Bergström *et al.*[20] used the IEC wind model, a traditional diabatic surface layer description, and proposed a wind model for wind flow over a forest. They found that the damage equivalent blade and tower loads for forest conditions are 35% larger than the IEC-A condition for all wind classes. Gontier *et al.*[21]

used the Kaimal, von Karman and Mann turbulence models suggested in the IEC guidelines as well as the Friedrich-Kleinhans model as a non-Gaussian turbulence model to compare fatigue loads of wind turbines. Their results show that the non-Gaussian Friedrich-Kleinhans model predicts loads that are significantly different from the loads obtained with the Kaimal model. Simulated winds by the non-Gaussian turbulence model have heavy tails resulting from the incremental distribution and, according to Gontier *et al.*[21], the form of the tails of the incremental distribution has a major influence on loads of the wind turbine and should be considered for fatigue analysis, see also Mücke *et al.*[22]. Gong and Chen[23] found for an operational turbine, with a Rayleigh distribution of mean wind speed, the long-term extreme of blade root edgewise bending moment was more sensitive than flap-wise bending moment to the non-Gaussian characteristics of the wind inflow. The extreme wind turbine responses to non-Gaussian wind inflow were considerably larger than the responses to Gaussian wind[23].

Few researchers have studied the structural loading of small wind turbines. Many of these have focussed on providing a method for fatigue life prediction of small wind turbine blades in the absence of long-term detailed operational data[24, 25]. In summary, although there is a considerable body of literature that investigates the effect of different terrains and wind models on fatigue loading of turbines, there is a gap in the literature in terms of loading of small wind turbines in highly turbulent sites.

This paper presents the results of simulating loads on a 10kW wind turbine in an urban site in Port Kennedy, Western Australia using the current NTM based on Kaimal turbulence power spectra. The results are compared with the prediction of turbine loads using the actual measured turbulence power spectral density at the Port Kennedy site. To make progress towards an improved turbulence model for non-open terrain sites, investigations are carried out on looking at the impact of modifying the Kaimal model using (1) measured standard deviation and (2) estimated integral length scale based on measured data.

2. Method

This study makes use of data collected from a wind monitoring system 5.94 m above the roof façade of a large warehouse belonging to the hardware chain Bunnings Ltd. in the suburb of Port Kennedy, Perth, Western Australia. The warehouse is a rectangular building, with its long-axis oriented NNE-SSW, with a very low pitched roof (almost flat). Extending above the roofline is a façade wall that surrounds the entire building such that the top of the wall is h = 8.5 m a.g.l. The building lies approximately 5 km distant from the coast (Indian Ocean) with the prevailing winds from the south-west. The warehouse is situated in a commercial estate but has no larger buildings or large trees in the vicinity. Within a 1 km radius of the site there are mainly residential buildings to the north and west, commercial and industrial buildings to the south and east. The south-west front and the north-west side are comparatively open, though street furniture and a car park exist on these sides[26]. Figure 2a shows the built-up area surrounding the Bunnings warehouse in Port-Kennedy, Western Australia and Figure 2b shows Building geometry around the Bunnings warehouse building and the anemometer location.

A Gill WindMaster Pro 3D ultrasonic anemometer was installed on a boom on a mast attached to the front-façade of the warehouse. The boom has a sliding collar in order to position the ultrasonic anemometer at different heights above the roof. The mast can be tilted

down in order to make adjustments or to replace sensors. The data consists of 10 Hz data over a 10-day period (between 12/08/2011 and 22/08/2011) measured at 14.44 m a.g.l (5.94 m above the roof façade). 10-day records have been extracted from one year worth of data in order to reduce processing time and make smaller files that could be stored.

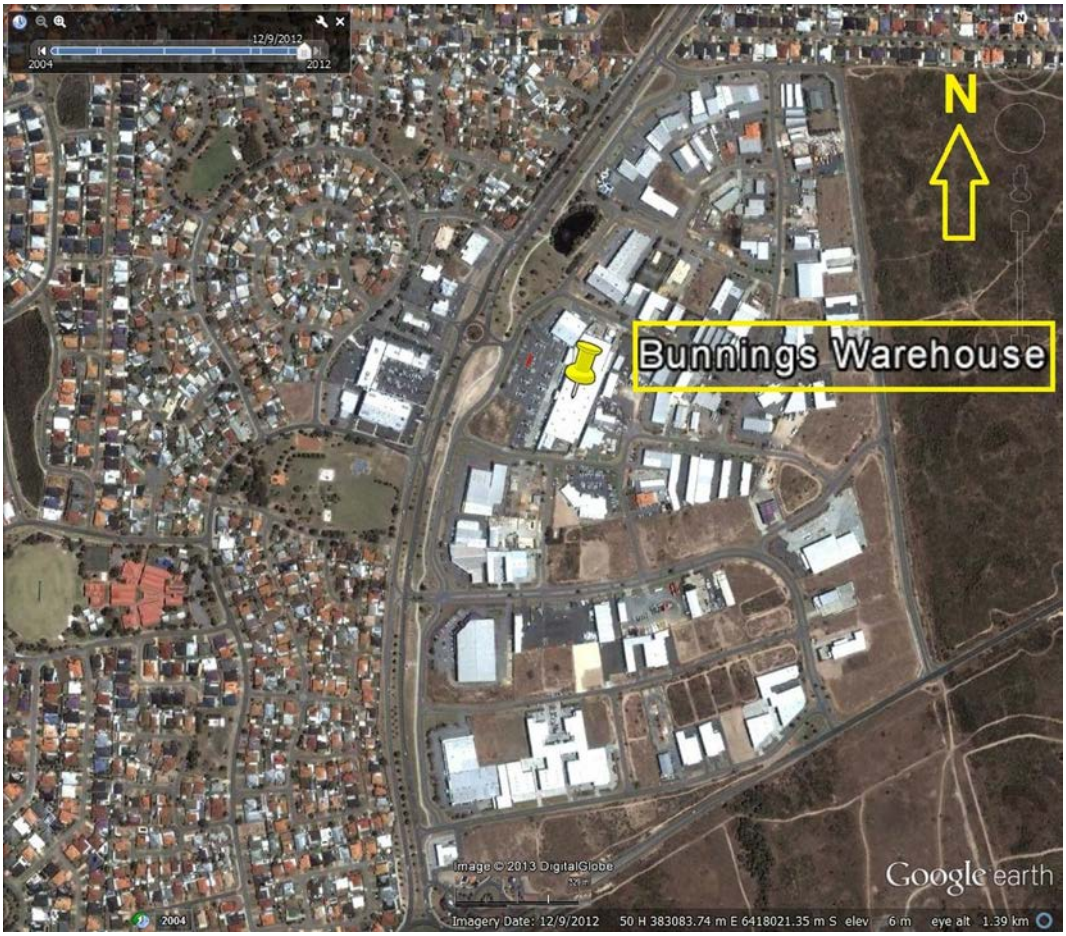

Figure 2a. The built-up area surrounding the Bunnings warehouse in Port-Kennedy, Western Australia

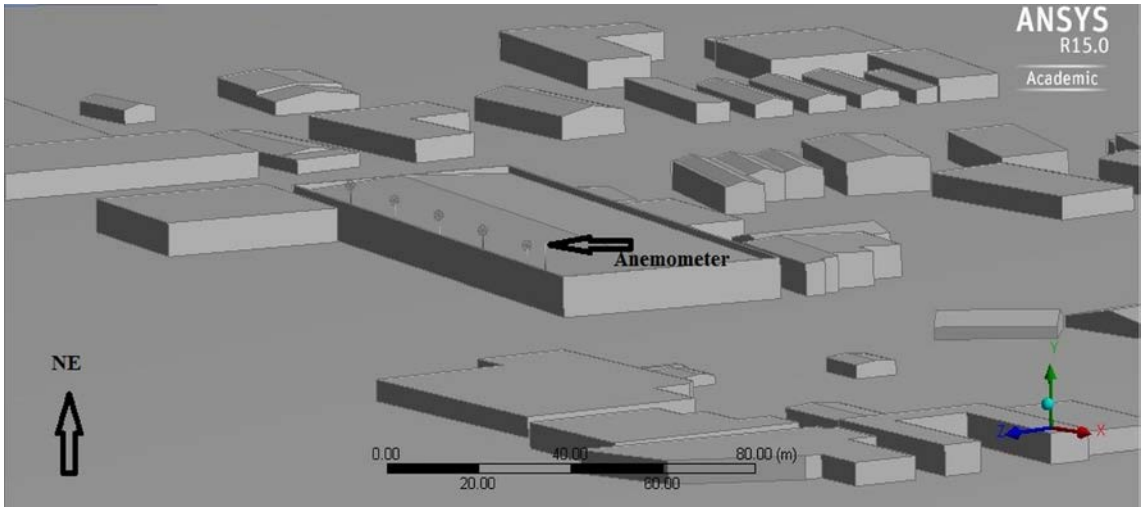

Figure 2b. Building geometry around the Bunnings warehouse building and the anemometer location

In the first stage, the stochastic turbulence simulator, TurbSim has been employed to simulate turbulent wind across the rotor of a 10 kW wind turbine for each of three scenarios (1) using the Kaimal turbulence power spectra as suggested in IEC61400-2 (In IEC61400-2, the component power spectral densities of the Kaimal model are defined in a non-dimensional form which is different from the general Kaimal spectra[9]) (2) using the measured turbulence power spectral density from the site, and (3) using a modified Kaimal turbulence power spectra. The 1-point measurements have been taken and used to provide a 3D wind field across the rotor by using TurbSim. The Kaimal model was modified in two ways: (1) using measured standard deviation and (2) using estimates of integral length scale based on measured data. The results have been repeated for a "typical" case and an "extreme" case, selected by the authors based on wind speed and standard deviation of wind speed, as explained in section 3.1. Note that extreme events cause ultimate load failure rather than fatigue failure, as defined in section 1. Some wind statistics of measured data and simulated data using the Kaimal turbulence power spectra have been presented first to show how the predicted values by the IEC standard differ from measured values at a highly turbulence site.

In the second stage, the aero-elastic code, FAST was used to generate load data for both typical and extreme cases by application of the wind fields produced by TurbSim for each of the three cases. Flap-wise bending moments at the roots of the turbine blades have been investigated to assess the effect of using the Kaimal spectra and its modified forms on predicting the structural loading of wind turbines. Some alternative codes to FAST, such as AeroDyn , Adams, Bladed and DHAT, can also be applied to generate load data. Buhl from the National Renewable Energy Laboratory in US and Manjock from Germanischer Lloyd WindEnergie in Germany have compared wind turbine aero-elastic codes which are commonly used for certification, such as Adams, DHAT, FAST and AeroDyn. They suggest that each code has its advantages and disadvantages but the differences in predictions from the different codes were within tolerance limits and certification bodies accept the use of the different codes in wind turbine design[27]. One key advantage of the TurbSIM/FAST method from the point of view of University researchers is that it is public domain code.

This work extends the previous work on modifying the Kaimal spectra to use more realistic integral length scales for the built environment[28]. The longitudinal integral length scale from the IEC standard (5.67z) is substituted by a more appropriate length scale for the built environment. This was derived from a sensitivity analysis of the Kaimal power spectra in comparison with length scales from measured data[28]. Lateral and vertical integral length scales are then estimated using ratios of length scales appropriate for the built environment (L_2/ L_1=0.5 and L_3/L_1=0.15) from a study by Christen *et al.* above the rooftop ($1<z/h<2$) of a street canyon[29]. The length scales in the built environment are much smaller than those of open terrain as obstacles in the built environment cause turbulent cascades of large scale eddies down to smaller scale eddies. The effect of reducing length scale is to shift the spectra towards reduced time scales i.e. higher frequency[28].

2.1 TurbSim

TurbSim, developed by US Department of Energy's National Renewable Energy Laboratory (NREL) is a stochastic, full-field, turbulent-wind simulator. This simulator applies a statistical model to numerically simulate a time series of three-component wind-speed vectors at points on a fixed, two-dimensional vertical rectangular grid[30]. Dynamic analysis software packages such as FAST[31], YawDyn[32], or MSC.ADAMS can use the output of

TurbSim as input data, where Taylor's frozen turbulence hypothesis has been utilized to obtain local wind speeds, interpolating the TurbSim-generated fields in both time and space[30].

Spectra of velocity components and spatial coherence are defined in the frequency domain, and a time series is produced by application of an inverse Fourier transform. A stationary process has been assumed as the underlying theory behind this method of simulating time series. Coherent turbulent structures can be superimposed onto the time series generated by TurbSim to simulate non-stationary components[30]. TurbSim allows the user to select a turbulence spectra model from default models or apply a numerical user-defined turbulence spectra and produces a 3D wind flow field with wind fluctuations governed by the spectra model.

2.2 FAST

NREL has also developed the FAST (Fatigue, Aerodynamics, Structures, and Turbulence) code, a comprehensive aero-elastic simulator which can predict both extreme and fatigue loads of two- and three-bladed horizontal-axis wind turbines (HAWTs). The FAST code can model the dynamic response of both two- and three-bladed, conventional, horizontal-axis wind turbines and uses the output of TurbSim to compute the loads on a selected wind turbine. The modelled wind turbine behaviour includes rotor-furling, tail furling, and tail aerodynamics, features that are useful in the analysis of most small wind turbines. During time-marching analyses, FAST makes it possible to model specific conditions such as extreme operating gust (EOG) or extreme wind direction change (EDC) and allows various options for controlling the turbine[31].

FAST includes two different forms of analysis modes. The first mode is time-marching of the nonlinear equations of motion. During this simulation wind turbine aerodynamic and structural response to wind-inflow conditions is specified with respect to time. Blade-element momentum (BEM) theory is used with FAST to compute aerodynamic forces on the blades. FAST has the capability to extract linearized representations of the complete nonlinear aero-elastic wind turbine. This capability is helpful for developing state matrices of a wind turbine "plant" to use in controls design and analysis[31].

In this paper, FAST has been used to simulate loading at the blade root of a 10 kW turbine over a period of ten minutes. The turbine modelled is the Small Wind Research Turbine (SWRT) of the US Department of Energy's National Wind Technology Centre (NWTC). SWRT is a three-blade, horizontal-axis machine with 5.8 m rotor diameter and is the smallest turbine with publicly available input data (such as aerofoil shape, blade geometry etc.) in the FAST archive[1]. A ten minute period was chosen for the simulation to ensure enough load cycles were captured.

It is worth noting that NREL researchers applied the FAST software to simulate the loading on a 10 kW turbine. The results suggested that the accuracy of FAST is questionable for prediction of small wind turbine tower loads at high wind speeds (18 m/s and above)[33]. Note that the current work deals with small wind turbine blade loads at wind speeds not greater than 12.67 m/s.

[1] https://nwtc.nrel.gov/FAST7

It is important to note that in this paper the authors are not modelling the SWRT machine installed on a rooftop. The aim of the work is to assess the loading on the SWRT at a highly turbulent site where the wind flow is affected by nearly obstacles to investigate the effect of turbulence on the structural loading of small wind turbines. Wind data from the roof of the warehouse in Port-Kennedy has been used purely to ensure that TurbSim will create a wind field that is three-dimensional and highly turbulent.

It is important to realise that the dynamic response of a small wind turbine in an urban site will be very different to that of a large wind turbine in a rural site. In addition to lower blade inertia for small wind turbines, the presence of obstacles in the urban environment will lead to a cascade of turbulence to smaller scales and higher frequencies. Compared to the large turbine in an open field, there is a greater possibility that the scales of turbulence the small wind turbine faces will be of a similar order to the dimensions of the turbine, and thus there is a greater possibility of dynamic resonance for the turbine.

3. Results and Discussion

3.1. Wind Statistics

Table 1 presents the statistics of ten days of three-dimensional measured data from the wind monitoring system on the warehouse. The table shows the mean, maximum, minimum and standard deviation of 10-minute mean wind speeds taken from three-dimensional data as well as standard deviation of longitudinal wind speeds over ten minutes observed during the ten-day period and how these parameters vary with wind direction.

Table 1
The statistics of ten-day measured data including mean, maximum, minimum and standard deviation of 10-minute mean wind speeds and standard deviation of longitudinal wind speed

Section	10-minute mean wind speeds				Standard deviation of longitudinal wind speed			Frequency (%)
	Mean (m/s)	Max. (m/s)	Min. (m/s)	Std. (m/s)	Mean (m/s)	Max. (m/s)	Min. (m/s)	
All Sectors	4.79	12.67	0.09	2.84	1.10	4.45	0.07	100
N	4.91	10.32	0.30	2.47	1.27	3.14	0.11	15.00
NE	2.43	5.36	0.43	0.82	0.52	1.54	0.12	24.72
E	1.55	2.35	0.18	0.41	0.28	0.75	0.07	5.28
SE	1.18	1.80	0.32	0.39	0.28	0.55	0.11	1.39
S	4.16	7.94	0.13	2.36	1.14	2.24	0.13	2.71
SW	7.04	12.02	0.99	2.25	1.86	3.20	0.21	8.47
W	6.32	11.52	0.09	2.52	1.38	3.06	0.19	18.96
NW	6.17	12.67	0.51	2.72	1.34	4.45	0.20	23.47

The table shows that across all wind sectors the average mean wind speed and average mean longitudinal wind fluctuation are around 5 m/s and 1 m/s, respectively. Thus a 10-minute

recording was selected that had these approximate values as a “typical” case. Across all sectors, the maximum mean wind speed and maximum longitudinal wind fluctuation are around 12.5 m/s and 4.5 m/s, respectively. Note that these values occurred in separate 10-minute recordings and Figure 1 was used to select an “extreme” case, where the mean wind speed was around 10.5 m/s and the wind fluctuation was 3.25 m/s. The extreme case is particularly of interest since they allow analysis of ultimate loads on the turbine. In this 10 day period, winds most frequently came from the NE and NW sectors. The greatest wind speeds, as well as wind fluctuations, were from the NW and N sectors and the SW and W sectors. Figure 2b shows the surrounding buildings to the Bunnings building as well as the location of the small wind turbines on top of the building. The results suggest that maximum levels of turbulence may originate from obstacles reasonably close to the ultrasonic anemometer including the turbine to the NNE and the façade wall immediately next to the anemometer to the NE, W, SW and S.

Figure 3 compares, for both the typical and extreme cases, the wind speed time series from measurement and from TurbSim simulation using the Kaimal power spectra from IEC61400-2. Table 2 presents the statistics of the wind speed time series and the turbulence intensities from measurement and from simulation for both the typical and extreme cases. For the typical case, the simulated time series shows greater turbulence intensity and a larger range of wind speeds compared to the measured data; the range of wind speeds lie between 2 and 8 m/s for the measured time series while for the simulated time series, wind speeds lie between 1 and 10 m/s. For the extreme case, the measured data show greater turbulence intensity and a larger range of wind speeds compared to the simulated data; the range of simulated wind speeds is between 4 and 17 m/s whereas for measured series wind speeds are between 3 and 22 m/s. Figure 4 shows the associated power spectra of longitudinal wind speed component for the measured and simulated flows for both typical and extreme cases. For the typical case, the simulated wind spectra over-estimate the turbulent power in the wind right across the spectrum. This is due to typically low speed, low power winds in the urban environment. For the extreme case there is a much better agreement between measured and simulated spectra although Figure 4 suggests that at lower frequencies there may be more energy in the turbulence in the measured data compared to the simulated data. One must be careful in drawing conclusions, however, because of the lack of data at low frequencies. The results indicate that use of an aero-elastic design code that incorporates the current Kaimal power spectra as defined in IEC61400-2, may over-estimate the turbulence intensity and power of the actual wind speeds experienced by a wind turbine in typical conditions in the built environment and may underestimate the turbulence intensity during extreme events.

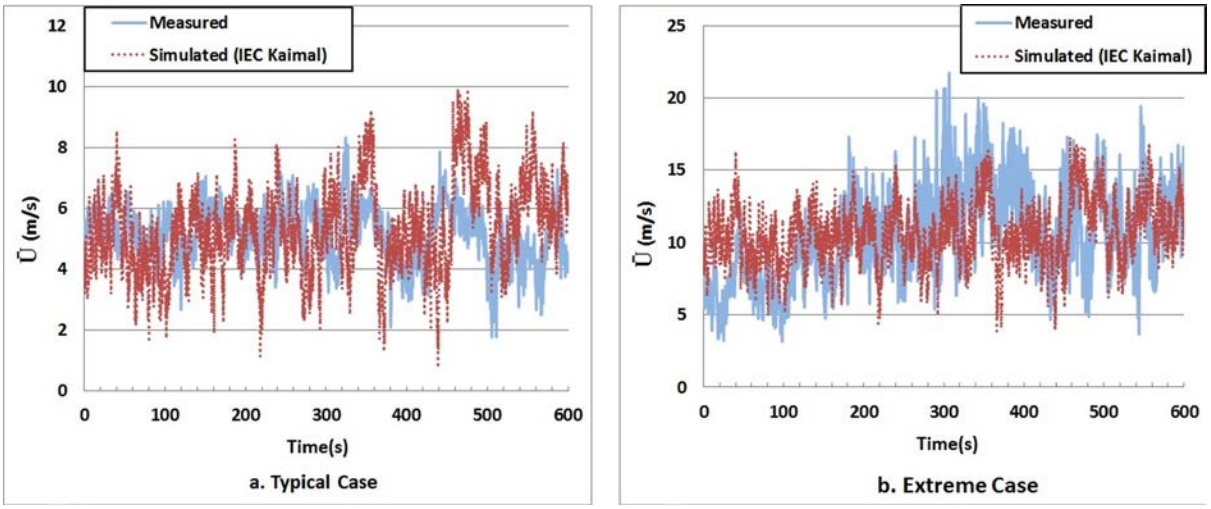

Figure3. Wind speed time series - 10 minutes of measured versus simulated data for typical and extreme cases

Table 2
The statistics of the wind speed time series from measurement and from TurbSim simulation using the Kaimal power spectra from IEC61400-2

Flow Type	Typical Case					Extreme Case				
	Mean (m/s)	Max. (m/s)	Min. (m/s)	Std. (m/s)	*I*	Mean (m/s)	Max. (m/s)	Min. (m/s)	Std. (m/s)	*I*
Measured	5.16	8.31	1.79	0.93	0.18	10.54	21.68	3.17	3.20	0.30
Simulated (IEC Kaimal)	5.36	9.90	0.76	1.44	0.27	10.72	17.27	3.88	2.12	0.20

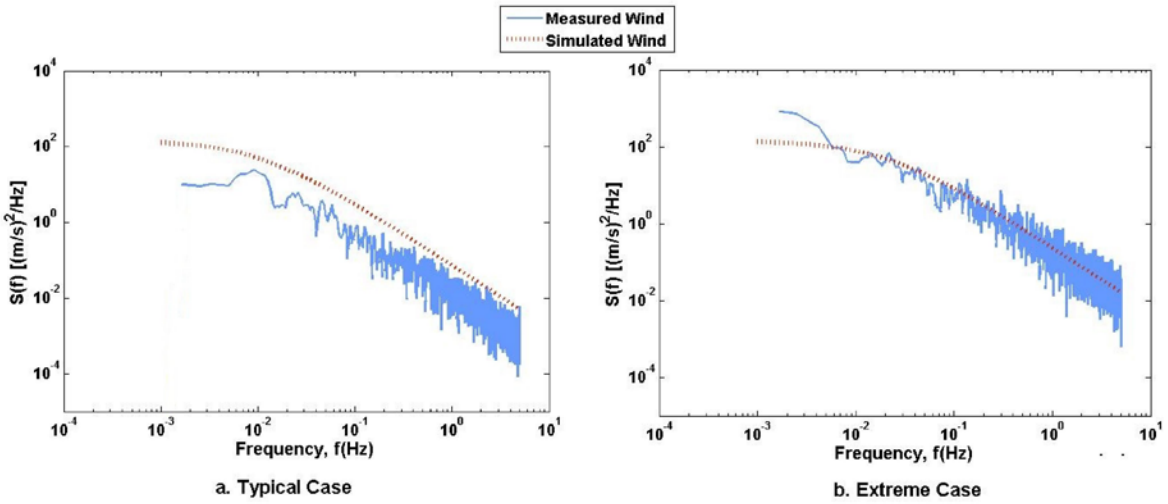

Figure4. PSD of longitudinal wind speed component for the measured and simulated flows for both typical and extreme cases

Wind speed increment statistics are useful descriptors of turbulence and the wind increment times series for time lag, τ, is given by:

$$U_\tau(t) = U(t+\tau) - U(t) \quad (4)$$

The increments directly evaluate the velocity difference after a characteristic time τ. Therefore, a large increment exceeding a specific threshold can be mentioned as a gust. In terms of a statistical analysis, there are points of interest that show how frequent a certain increment value occurs and whether this frequency depends on τ . The frequencies at which certain increments occur can be shown by plotting the probability density function (PDF) of $U_\tau(t)$. The tails of the PDF represent rare events corresponding to large wind increments. For small values of τ,, i.e. on small time scales, these extreme events can be attributed to wind gusts[34]. Some researchers have been applied wind speed increment statistics to investigate wind turbulence in semi-urban areas. The results of the research conducted by Sherry show a complicated relationship between stability and turbulence intermittency. The analysed data shows that the turbulence on small time scales is highly intermittent irrespective of atmospheric stability and can be predicted poorly by Gaussian statistics[35].

Figure 5 presents the PDFs of wind speed increment time series for measured and simulated data for both the typical and extreme cases. For each case, PDFs of Gaussian distributions with have been plotted on the same graph for comparison. Figure 5 clearly illustrates that for, both cases the PDF of the measured wind speed increments is non- Gaussian and have a special "heavy-tailed" shape where the heavy tails in the PDFs imply an increased probability of extreme events compared with a Gaussian distribution[36]. Not surprisingly the PDF for the simulated data, closely matches a Gaussian distribution since the NTM in IEC61400-2 assumes that the wind fluctuations have zero mean Gaussian statistics.

It is important that the extreme events of wind speed increments are included in the statistical description of the turbulence in the 3D wind fields used in aero-elastic models since short time wind speed increments (gusts) may cause important load situations. The PDFs can be parameterised such that the shape of the PDF can be determined by an intermittency parameter $\lambda^2(\tau)$, for which $\lambda^2 = 0$ means that the PDF has Gaussian shape and $\lambda^2 > 0$ that the PDF has heavy tails[34]. Note that analysing the statistics of wind data with this intermittency parameter is an additional independent aspect complementary to turbulence intensity and power spectra. Power spectra as scale dependent quantities correspond only to the width, i.e. standard deviation, of the PDFs of $U_\tau(t)$, which is not measured by λ^2. Figure 5 shows clearly that intermittent PDF with $\lambda^2 > 0$ can only be compensated partially by an increased standard deviation. For longer time series, i.e. more data, the tails of an intermittent PDF will always become larger than those of a Gaussian distribution.

Figure 6 shows a plot of intermittency parameter versus time lag for both typical and extreme cases. The figure reveals that $\lambda^2(\tau)$ for the simulated wind data is around zero for both cases, a property characteristic of Gaussian distributions, as expected. The measured data show greater intermittency values (heavy-tails in the PDFs of wind speed increments) for short time lags. As the time lag of the wind speed increment increases the PDF follows a Gaussian curve more closely. Figure 6 shows greater intermittency, on average, in the extreme case than in the typical case, and is expected from the greater variance in wind speeds in the extreme case. These results illustrate that there are significant non-Gaussian events occurring at this site due to wind gusts. This calls into question the extent to which the NTM of

IEC61400-2 is appropriate as a turbulence model for this type of site since it assumes wind components have zero-mean Gaussian statistics and does not use the higher-order statistics given by the PDF of wind speed increments. The fact that the synthetic time series fails to reproduce the measured behaviour cannot be ignored and represents an important weakness of the NTM in IEC61400-2, at least for this kind of non-open site and possibly for other types of terrain.

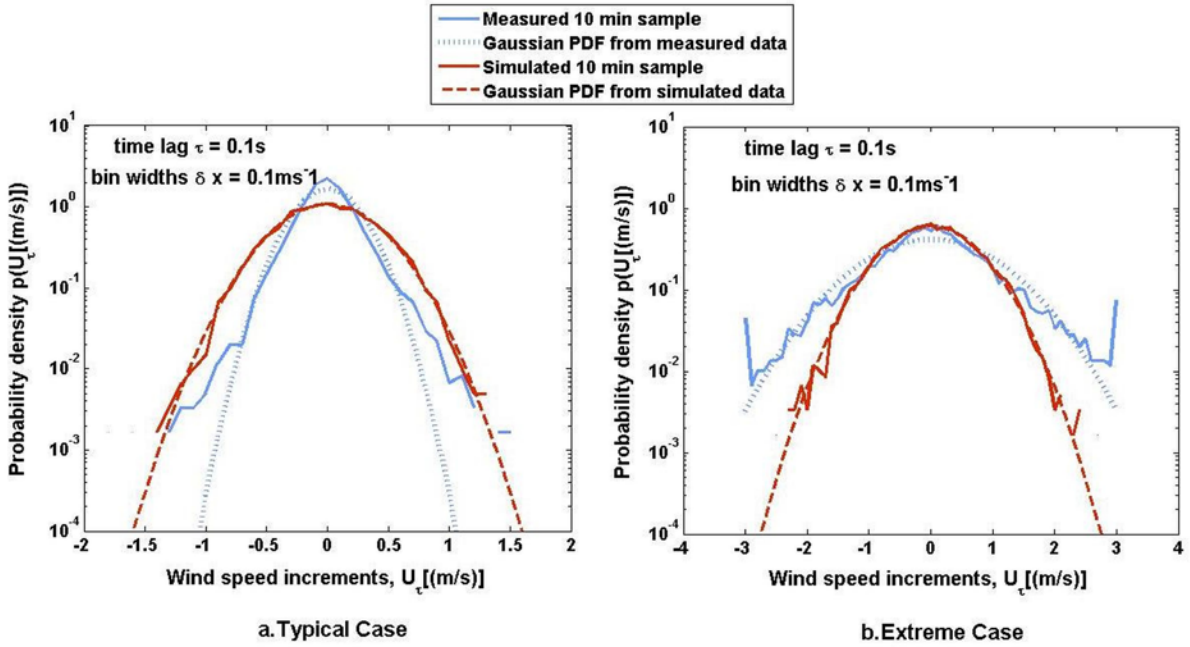

Figure 5. Examples of PDF of wind speed increments for measured and simulated 10-minute data.

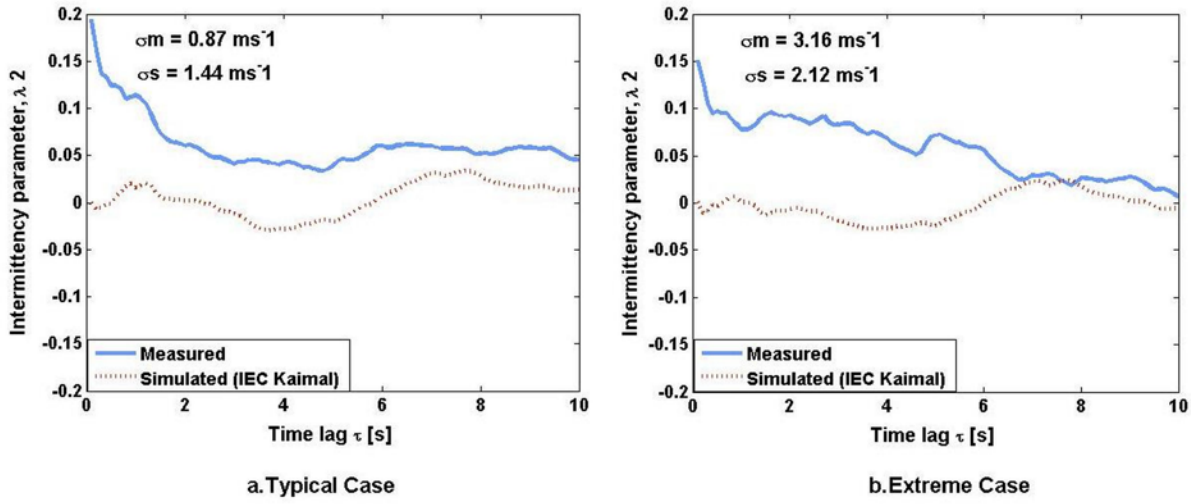

Figure 6. Intermittency parameter versus time lag for measured and simulated wind data

3.2. Loading

Figure7 presents the time series of the flap-wise bending moment at the root of blade 1 of the SWRT from the FAST simulation for the typical and extreme cases. Table 3 shows the statistics of the time series of the flap-wise bending moment from the FAST simulation for the typical and extreme cases. TurbSim has been used to simulate the 3D wind fields across the rotor using the IEC Kaimal turbulence power spectra (without modification) and the measured turbulence power spectral density. The 3D wind fields from TurbSim are then input into FAST. For the typical case, Figure 7 shows that use of the standard IEC Kaimal spectra over-estimates flap-wise bending moment at the root of the blade by around 20% compared to the use of measured spectra. The higher flap-wise moments may be explained by the fact that the NTM over-predicts the variance (and hence turbulence intensity) of wind speeds for the typical case (Figure 7a). The extreme case of Figure 7b shows reasonable agreement between use of measured and Kaimal spectra in the modelling with the notable exception of a few large events that FAST predicts when using the measured spectra. These events suggest that the maximum bending moments at the built environment site are around 60% greater than the maximum moments predicted by use of the current IEC61400-2 standard.

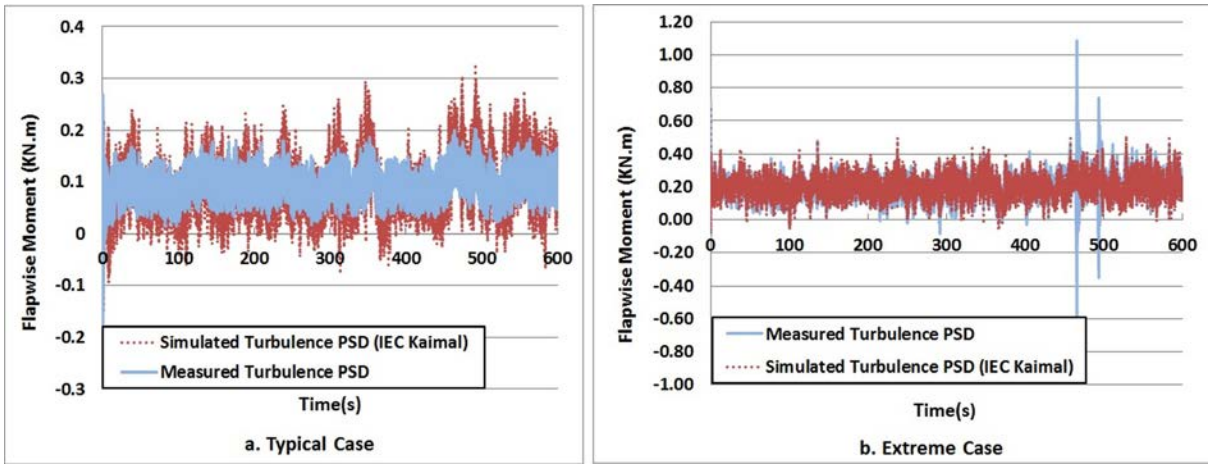

Figure 7. Flap-wise bending moment time series resulting from FAST simulations using Kaimal turbulence spectra versus measured turbulence spectra

Table 3
The statistics of the flap-wise bending moment time series resulting from FAST simulations using Kaimal turbulence spectra versus measured turbulence spectra.

Flow Type	Typical Case				Extreme Case			
	Mean (m/s)	Max. (m/s)	Min. (m/s)	Std. (m/s)	Mean (m/s)	Max. (m/s)	Min. (m/s)	Std. (m/s)
Measured Turbulence PSD	0.094	0.269	-0.215	0.033	0.201	1.080	-0.940	0.081
Simulated Turbulence PSD (IEC Kaimal)	0.088	0.329	-0.199	0.058	0.203	0.669	-0.084	0.077

Figure 8 shows the power spectral density (PSD) of the FAST time series of flap-wise bending moment at the root of blade 1 of the SWRT. The plots of PSD of flap-wise moment show the frequencies of wind excitation that lead to high bending moments on the root of the blade. Figure 8 shows that there is an area of increased power associated with bending moments at high frequencies greater than 1 Hz (short time scales). In the typical case it would appear that there a two peaks within this area of increased power, one centred around 2-3 Hz and one centred around 4-5 Hz. In the extreme case there appears to be just a single peak centred around 4 -5 Hz. At some revolution frequency, there appears to be resonance which creates blade flapwise vibration. The once per revolution frequency (1P) depends on the rpm of the machine, which will vary across the 10 minutes (particularly for the extreme case, where there is a large variation in wind speeds). Corbus and Meadors work on the SWRT suggest that this fundamental amplification in blade flap moment occurs around about 5Hz [37]. From Figure 7b, the measured turbulence PSD also suggests a peak around 5Hz, which coincides to an rpm of 300 rpm. In Figure 7a, there is a peak closer to 2Hz. Rather than saying that this peak has moved (between Figure 7a and 7b), it is more likely that the peak can be attributed to different forcing frequencies. In the typical case, the wind speeds are around 5m/s and the standard deviation is around 1 m/s. From Figure 20 of the report provided by Corbus and Meadors, the rpm is likely to be around 100 rpm[37]. In the extreme case, the wind speed is around 11 m/s and the standard deviation is around 3 m/s so from Figure 20 of the report provided by Corbus and Meadors[37], the rpm is likely to be around 150 – 350 rpm. Thus there will be incidences where the rpm is around 300 rpm and exciting flapwise vibration at around 5Hz. Since the flapwise bending moment on a blade is given by the product of the thrust force on the blade and the blade radius, it follows that the tower vibration could also show up in the flapwise PSD and therefore, the peak at 2Hz can also be due to tower resonance.

For the typical case in Figure 8a, the PSD of moments yields higher values and a broader peak for the use of the Kaimal spectra compared to use of the measured spectra in the TurbSim and FAST modelling. This is again likely to be due to the NTM predicting higher variance and turbulence intensity for the typical case. The extreme case shows a relatively good overall match between use of Kaimal and measured spectra although the measured data show greater variability and predict higher values than the Kaimal spectra modelling, particularly for frequencies between 0.1 to 5 Hz. This is expected since the measured data exhibits higher turbulence intensity than that predicted by the NTM, as shown in Figure 1.

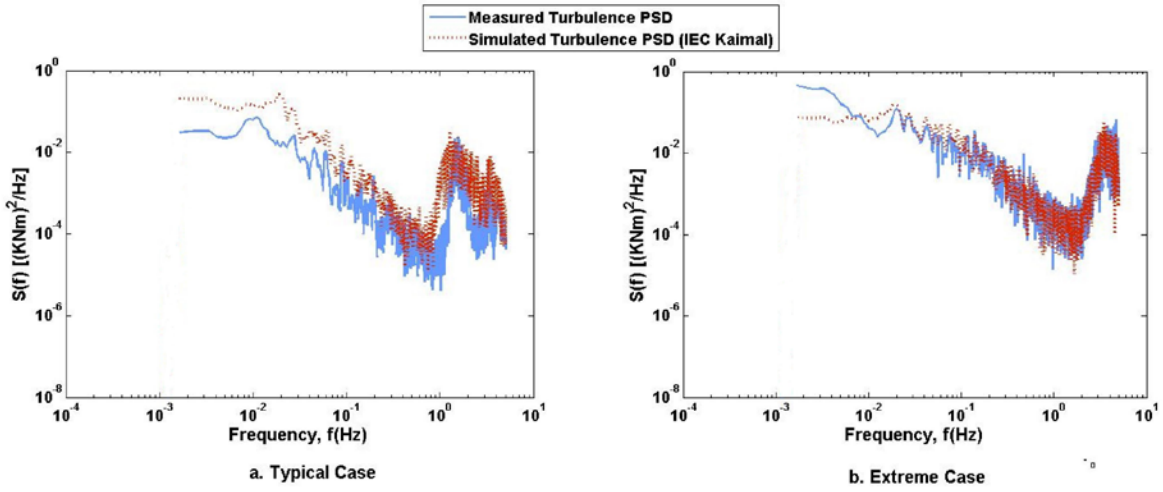

Figure 8. PSD of flap-wise bending moment from FAST simulations using Kaimal turbulence spectra versus measured turbulence spectra

3.3.Modification to the Standard NTM

The results of the previous section suggest that there is a need for a better turbulence model than the current NTM in the IEC61400-2 standard, especially to predict blade loading under extreme events, for those small wind turbine manufacturers who intend their turbines to be used in highly turbulent sites, such as the built environment. In attempting to improve the NTM this work uses the IEC standard Kaimal spectra as a starting point and investigates two approaches that involve modifying (1) the standard deviation of the longitudinal component of wind speed, and (2) the integral length scale. For both typical and extreme cases, Kaimal spectra have been modified by using values of parameters (1) and (2) that are more appropriate to the built environment site. As seen from Figure 1, the standard deviation of wind speed at this site is lower than that predicted by the NTM for the typical case and higher than that predicted by the NTM for the extreme case. In previous work[28], the authors assumed that the turbulence intensity and integral length scale can be modified independently of each other and conducted a sensitivity study to determine the integral length scale from measured data. It could be shown that the of longitudinal length scales of eddies at the Port Kennedy site were reduced by a factor of around four compared to the length scales assumed in the NTM[28]. This reduction in length scale is consistent with the cascading effect that obstacles in the built environment have on atmospheric turbulence whereby smaller eddies are generated.

Figure 9 shows the PSD of the flap-wise bending moment at the root of blade 1 of the SWRT FAST simulations using a modified Kaimal spectra where the standard deviation of wind speed in the Kaimal spectra has been adapted to reflect the measured wind speed standard deviation. The simulations were run for both typical and extreme cases and FAST simulations using the measured turbulence power spectral density have also been plotted for comparison. Figure 9, shows that the effect of making changes to the standard deviation of longitudinal wind speed in the Kaimal spectra shifts the PSD vertically on the graph. For the typical case, comparing Figure 8a with Figure 9a shows that the results using a turbulence model have been shifted downwards since the measured turbulence was lower than the NTM prediction (see Figure 1). The prediction now matches the measured PSD better, including the better agreement of the width of the peaks. In the extreme case, comparing Figure 8b and Figure 9b

shows that the results using the turbulence model have been shifted upwards since the measured turbulence was higher than the NTM prediction. Since the initial agreement in Figure 8b was reasonable, modifying the standard deviation for the extreme case has now resulted in over-prediction of the bending moments.

In Figure 10, the PSD of flap-wise bending moment at the root of blade 1 of the SWRT is shown and displays the results of FAST simulations using a modified Kaimal spectra where the integral length scale in the Kaimal spectra has been adapted to reflect the integral length scale predicted from measured data[28]. Again, the simulations were run for both typical and extreme cases and FAST simulations using the measured turbulence power spectral density have been also plotted for comparison. Figure 10 shows that the effect of making changes to the integral length scale in the Kaimal spectra shifts the PSD horizontally on the graph, with reduced length scale corresponding to a spectrum that is skewed to the right. For the typical case, comparing Figure 8a and Figure 10a, changing length scale clearly does not result in a better agreement between PSD values in the way that changing standard deviation did for the extreme case. Comparing Figure 8b and 10b, there is some evidence of better agreement of the PSD values around the top of the spectra, particularly in the range 0.1 to 5 Hz.

Table 4 summarizes the statistics of the time series of flap-wise bending moment from the FAST simulation as their PSD's shown in Figures 8, 9 and 10.Table 4 shows that for the typical case the modification of the Kaimal spectra using the measured wind speed standard deviation improves the results in terms of accuracy in agreement with the mean, maximum, minimum and standard deviation of the time series statistics. For the extreme case, the modification of the Kaimal spectra using the integral length scale predicted from measured wind data slightly improves the accuracy in terms of agreement with the maximum and standard deviation of the time series statistics.

Table 4
The statistics of the time series of flap-wise bending moment at the root of blade 1 of SWRT resulting from FAST simulations for the typical and extreme cases

Applied PSD to simulate 3D wind fields across the rotor	**Typical Case**				**Extreme Case**			
	Mean (kN.m)	Max. (kN.m)	Min. (kN.m)	Std. (kN.m)	Mean (kN.m)	Max. (kN.m)	Min. (kN.m)	Std. (kN.m)
Simulated Turbulence PSD (IEC Kaimal)	0.088	0.329	-0.199	0.058	0.203	0.669	-0.084	0.077
Simulated Turbulence PSD (IEC Kaimal with modified σ_u)	0.093	0.262	-0.209	0.039	0.194	1.350	-1.390	0.142
Simulated Turbulence PSD (IEC Kaimal with modified L)	0.091	0.315	-0.205	0.057	0.204	0.676	-0.083	0.081
Measured Turbulence PSD	0.094	0.269	-0.215	0.033	0.201	1.08	-0.940	0.081

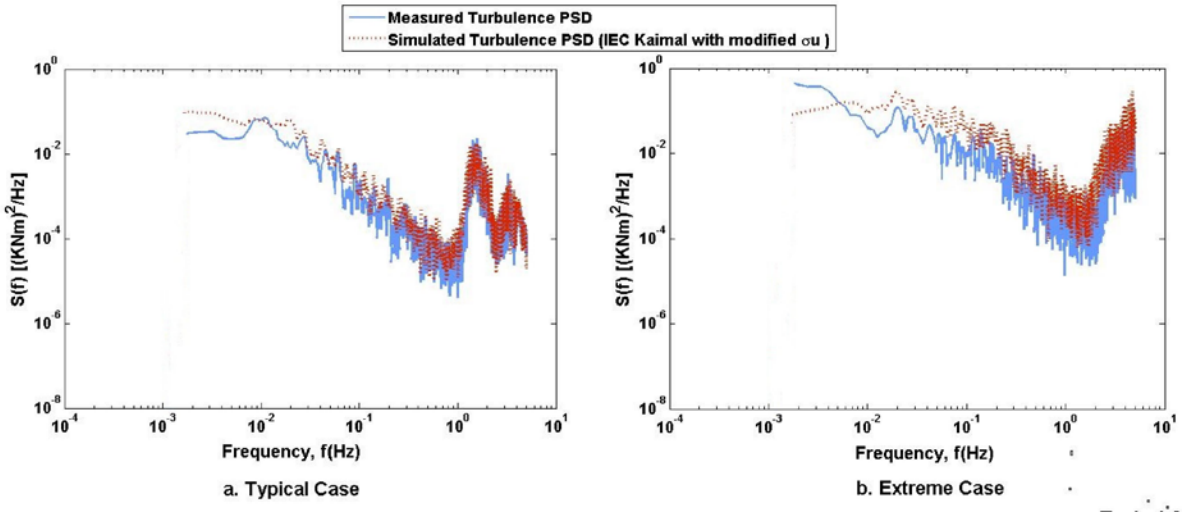

Figure 9. PSD of flap-wise bending moment from FAST simulation using Kaimal spectra (with modified σu) and measured turbulence spectra

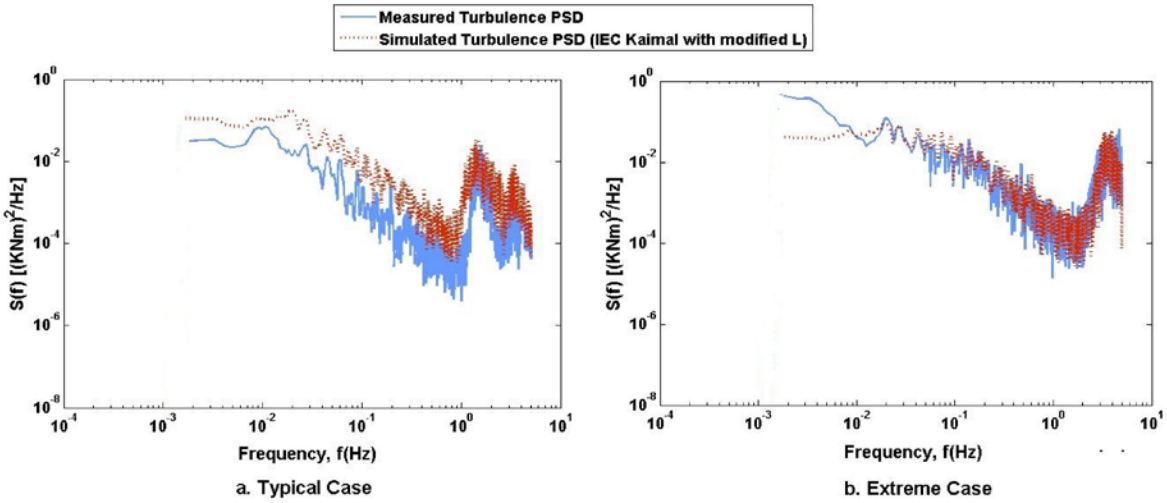

Figure 10. PSD of flap-wise bending moment from FAST simulation using Kaimal spectra (with modified length scale) versus measured turbulence spectra

For a typical wind speed, typical turbulence intensity case at a built environment site, Figures 8 - 10 support the findings of Riziotis and Voutsinas[6], which suggest that turbulence intensity is the dominant factor associated with loading and that small length scales are secondary factors. For the extreme case of high wind speed, high turbulence intensity at a built environment site, simply modifying the standard deviation of wind speed in the Kaimal spectra to try and obtain better agreement of the PSD of loads using the measured spectra is not as promising as for the typical case, and indicates that other factors need to be taken into account. This is not surprising as the results of section 3.1 showed that the extreme case has wind statistics that show very different characteristics to the typical case, including overall higher intermittency of wind over a wider range of time scales. Intermittency is linked with the heavy tails in a non-Gaussian distribution and the fact that the findings also showed large loading events in extreme winds supports the work of Gontier *et al.*[21], Mücke *et al.*[22],Gong and Chen[23], referred to section 1. There is some evidence that reducing the length scale in the Kaimal spectra results in an improved agreement between simulations using modelled and measured turbulence spectra and further research is required

to examine more cases within the Port Kennedy data set as well as data from different sites in the built environment. The limitations of this work include the fact that rooftop wind data has been used as an example of 3D, turbulent wind flow for simulations of a 10kW wind turbine that is not installed (nor intended to be installed) on a rooftop. Further work would aim to use wind data collected on a ground mounted monitoring mast in the built environment. In addition this work has only investigated flap-wise bending moments and further work is needed to consider other moments on the blade, particularly given the findings of Gong and Chen[23], mentioned in section 1.

4. Conclusion

The current IEC international design standard for small wind turbines, IEC61400-2, mandates designers to use the Normal Turbulence Model (NTM) incorporating a Kaimal turbulence power spectra in order to simulate 3D flow fields that are used to predict structural loading on small wind turbines. The current standard is based on wind turbines in open terrain and does not include a turbulence model for highly turbulent sites such as the built environment. This work attempts to address the research question of how accurate are the aero-elastic models that use the NTM in predicting the loading on turbines in non-open terrain. The aero-elastic code FAST was used to simulate flap-wise bending moments on the root of one blade of the 10kW NREL Small Wind Research Turbine. TurbSim software was used to produce the 3D wind fields to input into FAST, based on the Kaimal spectra and measured turbulence spectra from a built environment site at Port Kennedy, Western Australia. Two cases were considered: (1) a typical mean wind speed and turbulence intensity at the site, and (2) an extreme, high mean wind speed, high turbulence intensity at the site.

The findings, for the typical case, showed that using the Kaimal spectra in the TurbSim/FAST codes over-predicted flap-wise bending moment, although improvements in accuracy could be made by adjusting the standard deviation of longitudinal wind speed in the Kaimal spectra to reflect measured values. Whether a wind turbine designer would choose this approach would depend on whether it would lead to reduced structural costs for the blades, otherwise the over-predicted loads provide a safety factor in design.

The findings, for the extreme case, showed that using the Kaimal spectra produced reasonably similar results to using the measured spectra, with the exception of some large isolated loading events from the measured data that occurred on short time scales and were around double the maximum loads predicted by use of the current standard. This would be of more concern to the wind turbine designer and choice of safety factor would be critical. The work suggests the need for improvements to the NTM in order to model the non-Gaussian wind statistics that occur in extreme events such as sudden strong gusts. The work showed that some improvements in accuracy could be made by adjusting the integral length scale in the Kaimal spectra to reflect the smaller length scales of the built environment. Further research is required on different data sets before any recommendations can be made as to the characteristics of a turbulence model suitable for aero-elastic modelling of wind turbines in the built environment. Such a model would likely involve a new relationship between standard deviation and wind speed to replace equation 1 for highly turbulent sites as well as a non-Gaussian wind statistics associated with its turbulence power spectra. The development of such a model would be welcomed by small wind turbine manufacturers who intend their turbines to be used in highly turbulent sites, such as in urban areas.

Acknowledgements

The authors would like to acknowledge Bunnings Group Pty. Ltd. for allowing Murdoch University researchers to conduct the wind monitoring campaign at the Port Kennedy warehouse. The authors are also indebted to Mr. Simon Glenister for maintaining the monitoring system and collecting data. Mr. Amir Bashirzadeh Tabrizi would like to thank Murdoch University for the award of a post- graduate scholarship. Dr. Jonathan Whale would like to thank the Hanse-Wissenschaftskolleg Institute of Advanced Study in Germany for the award of a research fellowship. Prof. Joachim Peinke and Dr. Jonathan Whale would like to acknowledge Murdoch University for the Distinguished Collaborator Award that has funded research visits.

References

[1] RenewableUK, Small and medium wind UK market report.
[2] F. Balduzzi, A. Bianchini, L. Ferrari, Microeolic turbines in the built environment: Influence of the installation site on the potential energy yield, Renewable Energy, 45 (2012) 163-174.
[3] S.J. Ross, M.P. McHenry, J. Whale, The impact of state feed-in tariffs and federal tradable quota support policies on grid-connected small wind turbine installed capacity in Australia, Renewable Energy, 46 (2012) 141-147.
[4] http://www.bergey.com/technical/warwick-trials-of-building-mounted-wind-turbines.
[5]http://www.enhar.com.au/userfiles/file/Press%20releases/Enhar%20bulletin%20-%20Safety%20and%20reliability%20of%20micro%20and%20urban%20wind%20turbine%20installations%20in%20Australia.pdf.
[6] V.A. Riziotis, S.G. Voutsinas, Fatigue loads on wind turbines of different control strategies operating in complex terrain, Wind Engineering and Industrial Aerodynamics, 85 (2000) 211-240.
[7] L. Ledo, P.B. Kosasih, P. Cooper, Roof mounting site analysis for micro-wind turbines, Renewable Energy, 36 (2011) 1379-1391.
[8] W.D. Lubitz, Impact of ambient turbulence on performance of a small wind turbine, Renewable Energy, (2012) 1-5.
[9] International Electrotechnical Commission, IEC 61400-2,Wind turbines - Part 2: design requirements for small wind turbines, Third edition, in, Geneva, Switzerland, 2011.
[10] International Electrotechnical Commission, IEC 61400-2, Wind turbines-Part2: design requirements for small wind turbines,Second edition, in, Geneva, Switzerland, 2006.
[11] C.H.J. Stork, C.P. Butterfield, W. Holley, P.H. Madsen, P.H. Jensen, Wind conditions for wind turbine design proposals for revision of the IEC 1400-1 standard, Journal of Wind Engineering and Industrial Aerodynamics, 74-76 (1998) 443-454.
[12] M.M. Shokrieh, R. Rafiee, Simulation of fatigue failure in a full composite wind turbine blade, Composite Structures, 74 (2006) 332-342.
[13] H.J. Sutherland, N.D. Kelley, Fatigue damage estimated comparisons for northern European and U.S. wind farm loading environments, in: WindPower 95' AWEA, Washington, D.C.,USA, 1995.
[14] J.F. Mandall, D.D. Samborsky, D.S. Cairns, Fatigue of composite materials and substructures for wind turbine blades, in, Sandia National Laboratories, 2002.
[15] S. Lee, M. Churchfield, P. Moriarty, B.J. Jonkman, J. Michalakes, Atmospheric and wake turbulence impacts on wind turbine fatigue loading, in: 50th AIAA Aerospace Sciences Meeting, Tennessee, USA, 2012.
[16] K. Thomsen, P. Sorensen, Fatigue loads for wind turbines operating in wakes, Wind Engineering and Industrial Aerodynamics, 80 (1999) 121-136.
[17] M. Noda, R.G.J. Flay, A simulation model for wind turbine blade fatigue loads, Journal of Wind Engineering and Industrial Aerodynamics, 83 (1999) 527-540.

[18] G. Botta, M. Cavaliere, S. Viani, S. Pospisil, E¤ects of hostile terrains on wind turbine performances and loads: The Acqua Spruzza experience, Wind Engineering and Industrial Aerodynamics, 74-76 (1998) 419-431.
[19] F. Mouzakis, E. Morfiadakis, P. Dellaportas, Fatigue loading parameter identification of a wind turbine operating in complex terrain, Wind Engineering and Industrial Aerodynamics, 82 (1999) 69-88.
[20] H. Bergström, H. Alfredsson, J. Arnqvist, I. Carlén, E. Dellwik, J. Fransson, H. Ganander, M. Mohr, A. Segalini, S. Söderberg, Wind power in forests:Winds and effects on loads in, Elforsk, Stockholm, Sweden, 2013.
[21] H. Gontier, A. Schaffarczyk, D. Kleinnhaans, R. Friedrich, A comparison of fatigue loads of wind turbine resulting from a non-Gaussian turbulence model vs. standard ones, Journal of Physics: Conference Series, 75 (2007) 012070.
[22] T. Mücke, D. Kleinhans, J. Peinke, Atmospheric turbulence and its influence on the alternating loads on wind turbines, Wind Energy, 14 (2011) 301–316.
[23] K. Gong, X. Chen, Influence of non-Gaussian wind characteristics on wind turbine extreme response, Engineering Structures, 59 (2014) 727-744.
[24] J.A. Epaarachchi, P.D. Clausen, The development of a fatigue loading spectrum for small wind turbine blades, Journal of Wind Engineering and Industrial Aerodynamics, 94 (2006) 207-223.
[25] Y.J. Jang, C.W. Choi, J.H. Lee, K.W. Kang, Development of fatigue life prediction method and effect of 10-minute mean wind speed distribution on fatigue life of small wind turbine composite blade, Renewable Energy, (2014).
[26] A.B. Tabrizi, J. Whale, T. Lyons, T. Urmee, Performance and safety of rooftop wind turbines: Use of CFD to gain insight into inflow conditions, Renewable Energy, 67 (2014) 242-251.
[27] M.L.J. Buhl, A. Manjock, A comparison of wind turbine aeroelastic codes used for certification, in: 44th AIAA Aerospace Sciences Meeting and Exhibit, Reno, Nevada, USA, 2006.
[28] A.B. Tabrizi, J. Whale, T. Lyons, T. Urmee, Extent to which international wind turbine design standard, IEC61400-2 is valid for a rooftop wind installation, Wind Engineering and Industrial Aerodynamics, 139 (2015) 50-61.
[29] A. Christen, E. van Gorsel, R. Vogt, Coherent structures in urban roughness sublayer turbulence, International Journal of Climatology, 27 (2007) 1955-1968.
[30] B.J. Jonkman, TurbSim User's Guide: Version 1.50, in, NREL, Boulder, Colorado, USA, 2009.
[31] J.M. Jonkman, M.L.J. Buhl, FAST User's Guide, in, NREL, Boulder, Colorado, USA, 2005.
[32] D.J. Laino, A.C. Hansen, User's guide to the wind turbine dynamics computer program YawDyn, in, Windward Engineering LC, Salt Lake City, UT,USA, 2003.
[33] S. Dana, R. Damiani, J. van Dam, Validation of simplified load equations through loads measurement and modeling of a small horizontal-axis wind turbine tower, in, National Renewable Energy Laboratory (NREL), Golden, CO, USA, 2015.
[34] F. Boettcher, C. Renner, H.P. Waldl, J. Peinke, On the statistics of wind gusts, Boundary-Layer Meteorology, 108 (2003) 163-173.
[35] M. Sherry, The effect of stability on the intermittent nature of atmospheric winds, in: 33rd Wind Energy Symposium, Kissimmee, Florida, USA, 2015.
[36] A. Morales, M. Wächter, J. Peinke, Characterization of wind turbulence by higher-order statistics, Wind Energy, 15 (2012) 391-406.
[37] D. Corbus, M. Meadors, Small wind research turbine, in, NREL, Golden, Colorado, USA, 2005.